ELSEVIER

Evaluation of Six Methods for Extracting Relative Emissivity Spectra from Thermal Infrared Images

Zhao-Liang Li, F. Becker,*† M. P. Stoll* and Zhengming Wan‡*

An earlier version of this article was published in *Remote Sensing of Environment*, Vol. 69, No. 2, pp. 122–138. The current version completely supersedes the previously published version, which should be disregarded. The publishers apologize to the authors for the error.

The performance of six published methods for extracting relative spectral emissivity information from thermal infrared multispectral data has been evaluated. In the first part of this article, we recall those six methods and show mathematically that they are almost equivalent to each other. Then, using simulated data for the TIMS (Thermal Infrared Multispectral Scanner) instrument, we analyze the sensitivity of those methods to different sources of error which may occur in real data such as errors due to 1) method simplification, 2) instrumental noise and systematic calibration error, 3) uncertainties on the estimation of downwelling atmospheric radiance, and 4) uncertainties of atmospheric parameters in atmospheric corrections. In terms of resulting errors in relative emissivity, the results show that: a) all methods are very sensitive to the uncertainties of atmosphere. An error of 20% of water vapor in midlatitude summer atmosphere (2.9 cm) may lead to an error of 0.03 (rms) for Channel 1 (worst case) of TIMS. b) The effect of the atmospheric reflection term is very important. If this term is neglected in method development, this may lead to an error of 0.03 (rms) for Channel 1 and midlatitude summer atmosphere. This is the case for the alpha method. c) Instrumental noise commonly expressed by noise equivalent difference temperature (NEΔT) from 0.1 K to 0.3 K results in an error on relative emissivity ranging from 0.002 to 0.005 for all methods. d) Error on relative emissivity due to the instrumental calibration error (systematic error) is negligible. The study also shows that the relative emissivity derived with deviate atmosphere is linearly related to its actual value derived with correct atmospheric parameters. Based on this property, we propose three methods to correct for the errors caused by atmospheric corrections under horizontally invariant atmospheric conditions. A practical analysis with the real TIMS data acquired for Hapex-Sahel experiment in 1992 supports the results of this simulation. ©*Elsevier Science Inc., 1999*

INTRODUCTION AND OBJECTIVES

Investigation using thermal infrared (TIR) multispectral measurements has been undertaken over some decades to study the utility of those data for lithological mapping and mineral exploration. Numerous studies have demonstrated the great utility of spectral emissivity information extracted from those data for discrimination and sometimes identification of different types of surfaces (Vincent and Thomson, 1972; Kahle et al., 1980; Kahle and Goetz, 1983). Several new instruments are planed and/or approved for the next coming years, all having TIR bands, such as ASTER (Advanced Spaceborne Thermal Emission and Reflection Radiometer) and MODIS (Moderate Resolution Imaging Spectroradiometer) on

* LSIIT/CNRS(UPRESA-7005), Illkirch, France
† ISU, International Space University, Illkirch, France
‡ ICESS, University of California, Santa Barbara, California
Address correspondence to Z.-L. Li, GRTR/LSIIT, 5 Bd. Sebastien Brant, 67400 Illkirch, France. E-mail: li@sahel.u-strasbg.fr
Received 15 December 1998; revised 9 May 1999.

REMOTE SENS. ENVIRON. 69:197–214 (1999)

655 Avenue of the Americas, New York, NY 10010

0034-4257/99/$–see front matter
PII S0034-4257(99)00049-8

NASA's EOS-AM1 satellite. This will increase the number of TIR data available and will lead to the more and more researches using TIR data. Developments of algorithms to extract land surface temperature and emissivity from these new data have been recently undertaken (Wan and Snyder, 1996; Gillespie et al., 1996; 1998).

Such algorithms are very timely. In fact, the quantity measured remotely by a radiometer is the spectral radiance which depends not only on the surface parameters (surface emissivity and surface temperature) but also on the atmospheric parameters. Therefore, in order to extract the surface temperature and emissivity from space of aircraft data, it is necessary to perform both atmospheric corrections and a separation of surface emissivity and surface temperature contributions to the atmospherically corrected radiance. Unfortunately, these two problems are bound together due to the surface reflection. Furthermore, the separation of surface emissivity and temperature is very complicated because of the nonlinearity of the relationship between radiance and surface temperature. Moreover, regardless of the number of channels used in the measurement, there is always one more unknown than radiance measurements even if the quantities characterizing the atmosphere are known. Thus, for a radiometer having N channels, there are N values of spectral radiance, but $N+1$ unknowns [N emissivities (one per channel) plus one surface temperature], so that this system has no unique solution, unless complementary independent information is added.

If one is interested to extract both temperature and emissivity, different assumptions have to be made to reduce the number of unknowns, for example, the day/night method (Becker and Li, 1990; Watson, 1992a; Wan and Li, 1997), the grey body emissivity method (Barducci and Pippi, 1996), and the temperature–emissivity separation (TES) method (Gillespie et al., 1998). If one is interested only to determine spectral shape, relative emissivities are useful, and several methods have been proposed. These methods have been recently discussed by Gillespie et al. (1996). They are the reference channel method (Kahle et al., 1980), the emissivity normalization method (Gillespie, 1985), emissivity renormalization (Stoll, 1993), the temperature-independent spectral indices method (Becker and Li, 1990), the spectral ratio method (Watson, 1992b), and the alpha emissivity method (Kealy and Gabell, 1990). This article evaluates the performance of these six methods published in the literature. In the first part of this article, we shall recall the principle of these six methods. In the second part, using sets of simulated data, we analyze the sensitivity of those methods to different errors which may occur in real data. Based on this analysis, the last part will be devoted to the extraction of surface relative emissivities from TIMS (Thermal Infrared Multispectral Scanner) data acquired for Hapex-Sahel experiment in 1992 (Prince et al., 1995) and also to the discussion of results.

RELATIVE SPECTRAL EMISSIVITY INFORMATION EXTRACTION METHODS

Approximate Expression for the Channel Radiance

On the basis of radiative transfer equation, the radiance I_i measured from space or aircraft in Channel i may be written with a good approximation as (Becker and Li, 1990)

$$I_i = R_i \times \tau_i + R_{atti\uparrow}, \tag{1}$$

where τ_i is the channel total transmission of the atmosphere in Channel i, $R_{atti\uparrow}$ is the upwelling atmospheric radiance in Channel i, and R_i is the channel radiance observed in Channel i at ground level given by

$$R_i = \varepsilon_i B_i(T_s) + (1-\varepsilon_i) R_{atti\downarrow}. \tag{2}$$

In this expression, ε_i is the channel emissivity, $R_{atti\downarrow}$ is the downwelling hemispheric atmospheric radiance in Channel i, and $B_i(T_s)$ is the channel radiance which would be measured if the surface were a blackbody ($\varepsilon_i=1$) at temperature T_s, defined as

$$B_i(T_s) = \frac{\int_0^\infty f_i(\lambda) B_\lambda(T_s)\, d\lambda}{\int_0^\infty f_i(\lambda)\, d\lambda}, \tag{3}$$

in which $f_i(\lambda)$ is the spectral response of the radiometer in Channel i and $B_\lambda(T_s)$ is the Planck function given by

$$B_\lambda(T_s) = \frac{C_1}{\lambda^5 \left[\exp\left(\frac{C_2}{\lambda T_s}\right) - 1\right]} \tag{4}$$

with $C_1 = 1.191 \cdot 10^{-8}$ W/(m^2 sr cm^{-4}), $C_2 = 1.439$ cm K, and λ is the wavelength in centimeters.

Alternatively, the channel brightness temperature T_i and surface brightness temperature T_{gi} in Channel i can be used instead of the radiance I_i and R_i; they are respectively defined from I_i and R_i as

$$I_i = B_i(T_i), \tag{5a}$$

$$R_i = B_i(T_{gi}). \tag{5b}$$

Temperature-Independent Spectral Indices for Two Channels i and r ($TISI_{ir}$)

This method is based on the power law approximation of the Planck's function $B_i(T)$

$$B_i(T) = a_i T^{n_i}, \tag{5c}$$

where a_i and n_i are channel-specific constants for reasonable variation of temperature. Using this approximation, Becker and Li (1990; 1995) defined $TISI_{ir}$ for two Channels i and r (r being the reference channel) from the radiance R as

$$TISI_{ir} = \frac{C_r^{nir}}{C_i} \frac{a_r^{nir}}{a_i} \frac{R_i}{R_r^{nir}} = \frac{B_i(T_{gi}) - R_{atti\downarrow}}{B_i(T_g^{\max}) - R_{atti\downarrow}} \times \left(\frac{B_r(T_g^{\max}) - R_{atti\downarrow}}{B_r(T_{gr}) - R_{atti\downarrow}} \right)^{nir} \tag{6}$$

with

$$n_{ir}=\frac{n_i}{n_r}, \qquad C_k=\frac{1-\beta_k}{1-R_{atk\downarrow}/B_k(T_{gk})}, \qquad \text{and}$$

$$\beta_k=\frac{R_{atk\downarrow}}{B_k(T_s)}\cong\frac{R_{atk\downarrow}}{B_k(T_g^{\max})} \qquad (k=i,r)$$

in which $T_g^{\max}$ is the highest T_g among N channels used for a given pixel.

Considering Eqs. (5a), (5b), and (5c) and defining the downwelling atmospheric effective temperature $T_{a\downarrow}$ as

$$T_{a\downarrow}=\left(\frac{R_{atk\downarrow}}{a_k}\right)^{1/n_k}$$

it is easy to show from Eq. (6) that

$$TISI_{ir}\cong\frac{\varepsilon_i}{\varepsilon_r^{n_{ir}}}\left(1+\frac{T_g^{\max}-T_s}{T_s-T_{a\downarrow}}(n_{ir}-1)\right).$$

Since $T_g^{\max}$ and n_{ir} are respectively very close to T_s and unity, $T_s\gg T_{a\downarrow}$, the second term in the parenthesis in the above equation is very small and can be neglected, Therefore, TISI is almost independent of surface temperature and can be further approximated to

$$TISI_{ir}\cong\frac{\varepsilon_i}{\varepsilon_r^{n_{ir}}}.$$

If we take the channel having the highest T_g among N channel as reference channel r ($T_g^{\max}=T_{gr}$), from Eq. (6), and taking into account that

$$C_r=1 \quad \text{and} \quad B_i(T_g^{\max})=B_i(T_{gr})=(a_i/a_r^{n_{ir}})B_r(T_{gr})^{n_{ir}},$$

it is easy to check that

$$TISI_{ir}=\frac{B_i(T_{gi})-R_{ati\downarrow}}{B_i(T_g^{\max})-R_{ati\downarrow}}\cong\frac{\varepsilon_i}{\varepsilon_r^{n_{ir}}}. \tag{7}$$

Reference Channel Method (REF)

The reference channel method was first developed by Kahle et al. (1980). This method assumes that the emissivity in one channel, for example, Channel r, ε_r, has a constant value $\varepsilon_r^{\#}$ for all pixels, that is, $\varepsilon_r=cst=\varepsilon_r^{\#}$. Considering channel r for which $\varepsilon_r=\varepsilon_r^{\#}$ and knowing atmospheric parameters (τ_r, $R_{atr\uparrow}$, and $R_{atr\downarrow}$), an approximate surface temperature $T_s^{\#}=T_s(\varepsilon_r^{\#})$ can be derived for each pixel from its measured radiance, I_r, by the inversion of Eqs. (1), (2) and (3), that is,

$$T_s^{\#}=T_s(\varepsilon_r^{\#})=B_r^{-1}\left[\frac{I_r-R_{atr\uparrow}-(1-\varepsilon_r^{\#})R_{atr\downarrow}\tau_r}{\tau_r\varepsilon_r^{\#}}\right]$$

$$=B_r^{-1}\left[\frac{B_r(T_{gr})-(1-\varepsilon_r^{\#})R_{atr\downarrow}}{\varepsilon_r^{\#}}\right]. \tag{8}$$

This temperature is then used with Eqs. (1) and (2) to derive emissivity values for the remaining channels, that is,

$$\varepsilon_i^{\#}=\varepsilon_i(\varepsilon_r^{\#})=\frac{(I_i-R_{ati\uparrow})/\tau_i-R_{ati\downarrow}}{B_i(T_s^{\#})-R_{ati\downarrow}}=\frac{B_i(T_{gi})-R_{ati\downarrow}}{B_i(T_s^{\#})-R_{ati\downarrow}}. \tag{9}$$

In order to study the sensitivity of $\varepsilon_i^{\#}$ on $\varepsilon_r^{\#}$, the chosen value of ε_r, we insert Eq. (8) into (9) and taking into account Eq. (5c), one gets by a simple mathematical manipulation that

$$\frac{\varepsilon_i^{\#}}{(\varepsilon_r^{\#})^{n_{ir}}}=\frac{TISI_{ir}^{wa}(1-\gamma_i)}{(1-TISI_{ir}^{wa}\gamma_i)+(TISI_{ir}^{wa}\gamma_i-\gamma_r)(1-(\varepsilon_r^{\#})^{n_{ir}})} \tag{10}$$

with

$$\gamma_k=\frac{R_{atk\downarrow}}{R_k}=\frac{R_{atk\downarrow}}{B_k(T_{gk})} \qquad (k=i,r)$$

and

$$TISI_{ir}^{wa}=\frac{a_r^{n_{ir}}}{a_i}\times\frac{R_i}{R_r^{n_{ir}}}=\frac{B_i(T_{gi})}{B_i(T_{gr})}=\left(\frac{T_{gi}}{T_{gr}}\right)^{n_i},$$

which is equivalent to $TISI_{ir}$ if the atmospheric reflection term [last term in Eq. (2)] were neglected in $TISI_{ir}$. Since $TISI_{ir}^{wa}\ \gamma_i\cong\gamma_r$ and $\varepsilon_r^{\#}$ is close to unity, the second term in the denominator of Eq. (10) is very small compared with the first term and can be neglected in a first-order approximation. This demonstrates that if we divide $\varepsilon_r^{\#}$ derived from Eq. (9) by $(\varepsilon_r^{\#})^{n_{ir}}$, the quantity obtained is almost independent on the value of emissivity in reference channel r ($\varepsilon_r^{\#}$) given in Eq. (8), particularly when actual ε_r is close to unity. That is to say,

$$\frac{\varepsilon_i^{\#}}{(\varepsilon_r^{\#})^{n_{ir}}}\cong\frac{\varepsilon_i}{\varepsilon_r^{n_{ir}}}.$$

This is the case for emissivity normalization method in which we choose the channel having the highest emissivity value among N channels for a given pixel as a reference channel r. Under this condition, Eq. (10) can be simplified to

$$\frac{\varepsilon_i}{\varepsilon_r^{n_{ir}}}\cong\frac{\varepsilon_i^{\#}}{(\varepsilon_r^{\#})^{n_{ir}}}\cong\frac{TISI_{ir}^{wa}(1-\gamma_i)}{1-TISI_{ir}^{wa}\gamma_i}=\frac{B_i(T_{gi})-R_{ati\downarrow}}{B_i(T_{gr})-R_{ati\downarrow}}. \tag{11}$$

This shows that two methods (TISI and emissivity normalization method) are equivalent to the first order.

Emissivity Normalization Method (NOR)

This method was first described by Gillespie (1985) and used by Realmuto (1990) and Gillespie et al. (1998). This method assumes a constant emissivity in all N channels for a given pixel, which enables N temperatures to be calculated for each pixel using (8) from their radiance. The maximum of those N temperatures ($T_g^{\max}$) is considered to be the land surface temperature (T_s) and used to derive emissivity values for the other channels as it is done with the REF method. If the maximum of temperatures for a given pixel occurs in Channel k (k may be one of the channels between 1 and N), this means that the emissivity in Channel k is the maximum for this pixel. As for the REF method, the derived emissivity value was divided by $\varepsilon_k^{n_{ir}}$ for other Channels i is almost independent on the given ε_k value as described by Eq. (11).

Emissivity Renormalization Method (RE)

This method, similar to two-channel TISI method, was first developed by Stoll (1993). Besides the approximations made in constructing TISI, this method assumes further that

$$TISI_{ij} \cong \frac{\varepsilon_i}{\varepsilon_j} \qquad \text{instead of} \qquad \frac{\varepsilon_i}{\varepsilon_j^{nij}},$$

where j denotes the channel having the maximum of temperature among N channels for a given pixel: $T_g^{\max}=T_{gj}$.

This is a good approximation because both ε_j and n_{ij} are close to unity for thermal infrared instruments provided that the positions of Channels i and j are not too far. This is the case for TIMS instrument.

Based on this approximation, Stoll (1993) constructed another spectral index, called RE, such as

$$RE_i = \frac{TISI_{ij}}{(1/N)\sum_{k=1}^{N} TISI_{kj}}, \qquad \text{which means}$$

$$RE_i \cong \frac{\varepsilon_i}{(1/N)\sum_{k=1}^{N} \varepsilon_k}. \tag{12a}$$

It should be noted that the average of RE_i for N channels is equal to unity, that is,

$$\frac{1}{N}\sum_{i=1}^{N} RE_i = 1,$$

which permits us to compare the spectral emissivity ε_i in relation to its mean for N channels, and therefore to study directly the spectral variations of emissivity.

To compare directly with other methods, if we choose the Channel r as a reference channel, the relative emissivity in Channel i with respect to this channel is straightforwardly obtained by taking the ratio of the two REs defined by Eq. (12a), that is, Eqs. (12b) and (12c):

$$\frac{\varepsilon_i}{\varepsilon_r} = \frac{RE_i}{RE_r}, \tag{12b}$$

which means that

$$\frac{\varepsilon_i}{\varepsilon_r} = \frac{TISI_{ij}}{TISI_{rj}} = \frac{B_i(T_{gi}) - R_{atiu}}{B_i(T_g^{\max}) - R_{atiu}} \times \frac{B_r(T_g^{\max}) - R_{atru}}{B_r(T_{gr}) - R_{atru}} \qquad \text{with}$$

$$T_g^{\max} = T_{gj} \tag{12c}$$

Spectral Ratio Method (SR)

This method was proposed by Watson (1992b) based on the concept that, although the spectral radiances are very sensitive to small changes in temperature, the ratios are not. Taking the spectral ratios of two radiances given in Eq. (2) for two channels i and r (r being the reference channel), the emissivity ratios can be determined from

$$\frac{\varepsilon_i}{\varepsilon_r} = \frac{B_i(T_{gi}) - R_{atiu}}{B_r(T_{gr}) - R_{atru}} \times \frac{B_r(T_s) - R_{atru}}{B_i(T_s) - R_{atiu}}$$

provided that surface temperature (T_s) is known. Watson (1992b) demonstrated that the maximum value of the surface brightness temperatures among N channels ($T_g^{\max}$) represents a best estimate of the surface temperature.

In consequence, he suggested to replace T_s by $T_g^{\max}$ in above equation. In this manner, the SR method gives exactly the same emissivity ratios as the RE method [Eq. (12c)].

Alpha Emissivity Method (α)

This method was developed by Kealy and Gabell (1990) based on the Wien's approximation of the Planck function given by Eq. (4). Taking natural logarithms of the radiance $B_i(T_s)$ given by Wien's approximation and eliminating the surface temperature T_s by subtracting natural logarithms of one channel from its mean for N channels, and defining α for Channel i such that

$$\alpha_i = \lambda_i \ln \varepsilon_i - \frac{1}{N}\sum_{k=1}^{N} \lambda_k \ln \varepsilon_k, \tag{13a}$$

Kealy and Gabell (1990) showed that

$$\alpha_i = \lambda_i \ln B_i(T_{gi}) - \frac{1}{N}\sum_{k=1}^{N} \lambda_k \ln B_k(T_{gk}) + K_i$$

where K_i is a constant value which can be calculated from the channel wavelengths and the first radiation constant (Kealy and Gabell, 1990). This means that α_i can be directly obtained from the measured radiance $B_i(T_{gi})$.

It should be noted that this method is difficult to use when dealing with the measured radiance R_i or I_i because the surface reflection term [last term in the right-hand side of Eq. (2)] is neglected in constructing α_i. As for RE method, after a simple mathematical manipulation of Eq. (13a), the relative emissivity in Channel i with respect to reference channel r can be easily obtained by Eq. (13b):

$$\frac{\varepsilon_i}{\varepsilon_r^{nir}} = (\exp(\alpha_i - \alpha_r))^{1/\lambda_i}. \tag{13b}$$

SENSITIVITY ANALYSIS FOR DIFFERENT METHODS WITH SIMULATED TIMS DATA

We shall analyze in this section the sensitivity of those methods to different sources of errors which may occur in real data such as errors due to

a. method simplification,
b. instrumental noise and calibration error,
c. uncertainties on the estimation of downwelling atmospheric radiance,
d. uncertainties of atmospheric parameters in atmospheric corrections.

The Simulated Data Sets

In order to evaluate the different methods described above, four data sets of thermal infrared radiance were

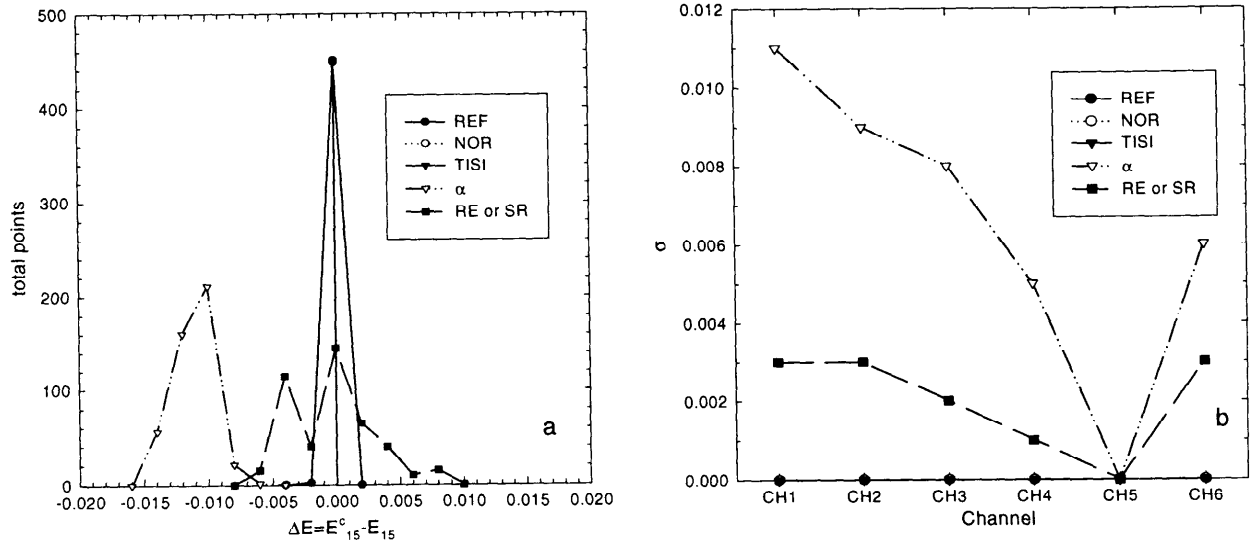

Figure 1. Error of relative emissivity resulting from the model simplifications: a) histogram of the difference between E'_{15} derived from radiance by the six methods and E_{15} computed directly by ratio of emissivity values [eq. (14)]; b) standard deviation of $E'_{i5}-E_{i5}$ for different channels of TIMS.

simulated for the TIMS (Thermal Infrared Multispectral Scanner; Palluconi and Meeks, 1985) radiometer (the TIMS has six spectral channels in 8–12 μm. The center positions of each of channels are 8.379 μm, 8.782 μm, 9.178 μm, 9.878 μm, 10.711 μm, and 11.637 μm). Each data set was created for a variety of natural Earth surface materials with five surface temperatures varying from 290 K to 310 K in steps of 5 K. Ninety types of natural surface materials including igneous, metamorphic, and sedimentary rocks, desert varnish, soils, vegetation, water, and ice were considered in this analysis. The channel emissivity for each material was determined from the hemispherical spectral reflectance measured by Salisbury and D'Aria (1992) and by F. Nerry (personal communication, 1996). The channel radiance for different data sets were synthesized for each material at a given surface temperature as following:

Data Set for Radiance at Surface Level without Atmospheric Reflection

To evaluate the sensitivity of different methods to the error resulting from method simplification, we simulated the channel radiance emitted directly by surface materials at surface level using the formula:

$$R_i^j = \varepsilon_i^j B_i(T_s),$$

where R_i^j would be the channel radiance at ground level in Channel i (i=1–6 for TIMS) for material j (j=1–90) if there were no atmosphere and ε_i^j is the channel emissivity determined from the laboratory measurements.

Table 1. The Maximum Absolute Error of Emissivity Ratio and the Standard Deviation of Emissivity Ratio Error for Different Methods Due to Both the Model Simplification and the Instrumental Noises

		*NE*ΔT			
		0.1 K		*0.3 K*	
Channels	*Methods*	*Max Error*	σ	*Max Error*	σ
1	REF	0.005	0.002	0.012	0.005
	NOR	0.005	0.002	0.012	0.005
	TISI	0.005	0.002	0.012	0.005
	ALPHA	0.017	0.011	0.023	0.012
	RE or SR	0.013	0.004	0.015	0.005
4	REF	0.003	0.001	0.010	0.004
	NOR	0.003	0.001	0.010	0.004
	TISI	0.003	0.001	0.009	0.004
	ALPHA	0.008	0.005	0.014	0.006
	RE or SR	0.006	0.002	0.011	0.004

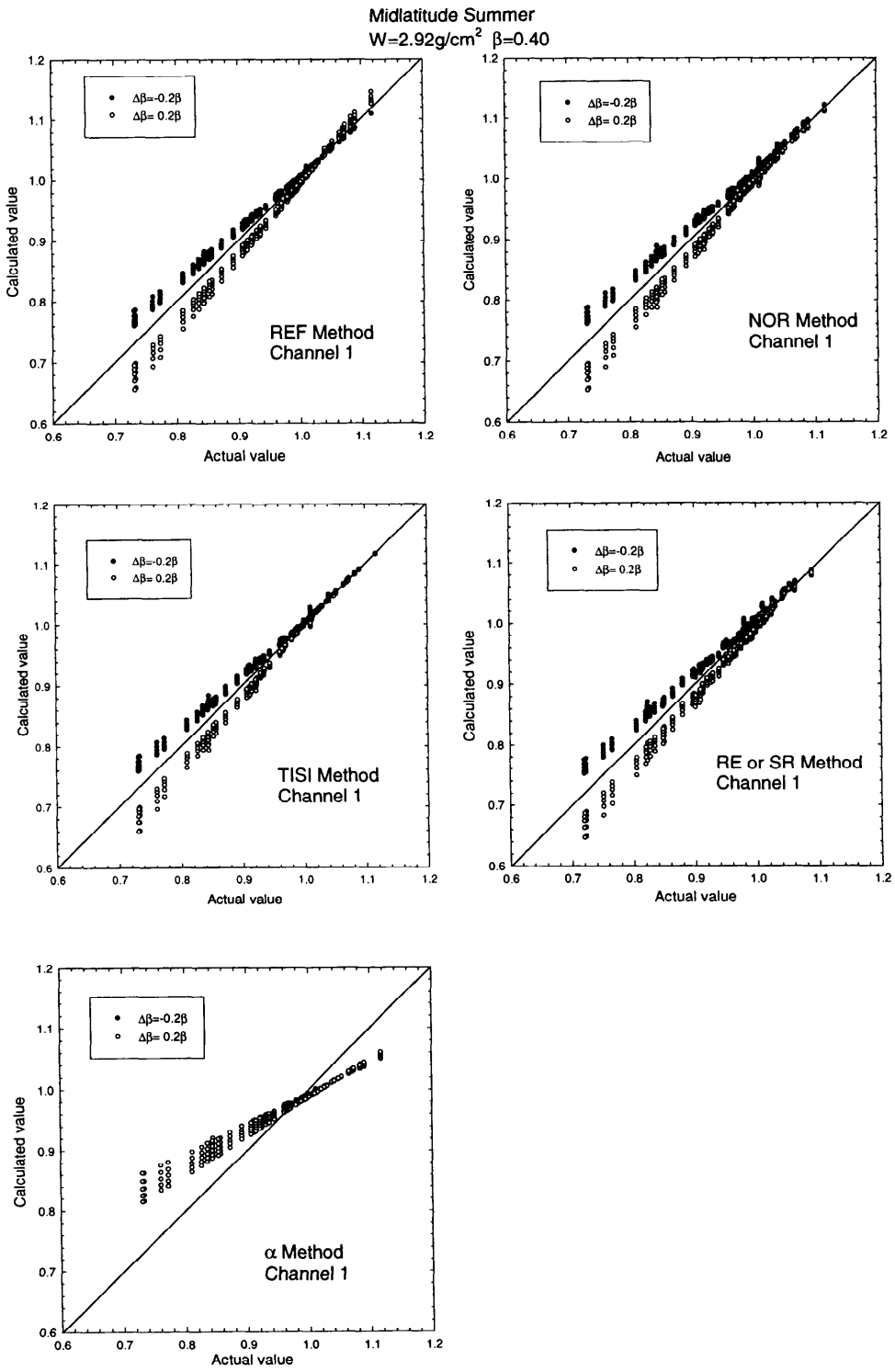

Figure 2. Effect of downwelling atmospheric radiance error on relative emissivity calculation. The abscissa represents the actual value E_{15} computed directly using emissivity values while the ordinate represents E'_{15} calculated from the simulated radiance with an error of ±20% on the actual downwelling atmospheric radiance.

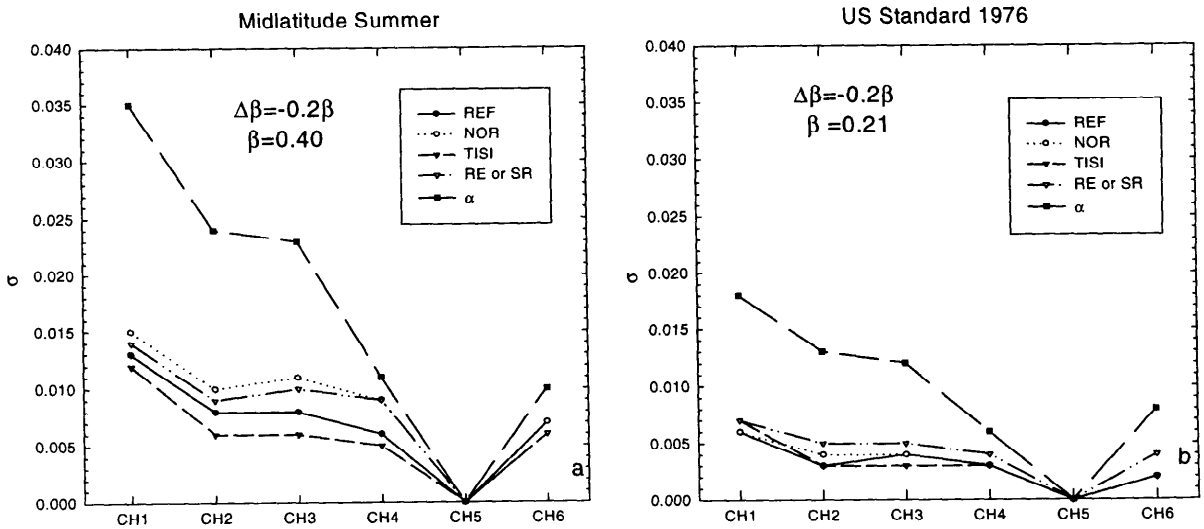

Figure 3. Standard deviation of $E_{i5}^{c}-E_{i5}$ versus TIMS channels for two types of atmosphere: a) midlatitude summer; b) U.S. standard 1976.

Data Set Including the Instrument Noise and Systematic Calibration Error

To study the sensitivity of different methods to the errors caused by instrumental noise and by systematic calibration error, we simulate the radiance by keeping the same surface parameters as that in the previous subsection, but changing NEΔT (noise equivalent temperature difference) and ΔT_c (systematic instrument calibration error) values as below:

a. NEΔT=0.1 K, ΔT_c=0 K;
b. NEΔT=0.3 K, ΔT_c=0 K;
c. NEΔT=0.1 K, ΔT_c=1 K;
d. NEΔT=0.3 K, ΔT_c=1 K.

Data Set for Radiance at Surface Level

To analyze the sensitivity of different methods to the error of downdwelling atmospheric radiance, we first calculated R_{atil} using Modtran 3.5 (Kneizys et al., 1996) with two types of atmosphere given by Modtran; midlatitude summer and U.S. standard atmospheric profiles. Note that the total column water vapor content W for the midlatitude summer profile is 2.92 g/cm^2, whereas for the U.S. standard profile W=1.42 g/cm^2. Then the radiance R_i at ground level is simulated for six channels of TIMS by Eq. (2) with the same variations of surface temperature and emissivity for the two preceding simulations.

Data Set for Radiance at Satellite or Aircraft Level

To study the sensitivity of different methods to the error of uncertainties of atmosphere in atmospheric correction, instead of simulating R_i at ground level for TIMS as we did in the previous subsection, we simulated the radiance measured at satellite level, I_i using Eqs. (1) and (2). The atmospheric quantities required in constructing I_i are

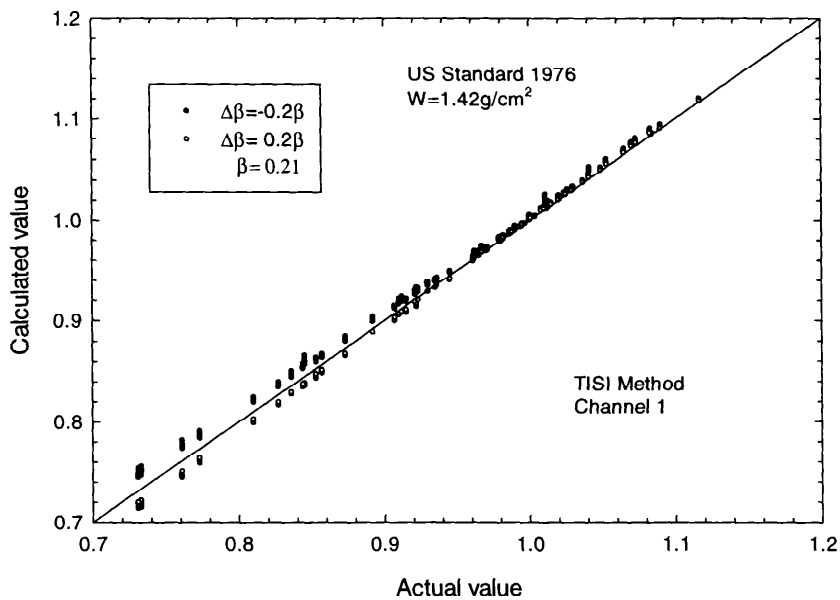

Figure 4. Same as Figure 2 but for U.S. standard atmosphere 1976 and TISI method.

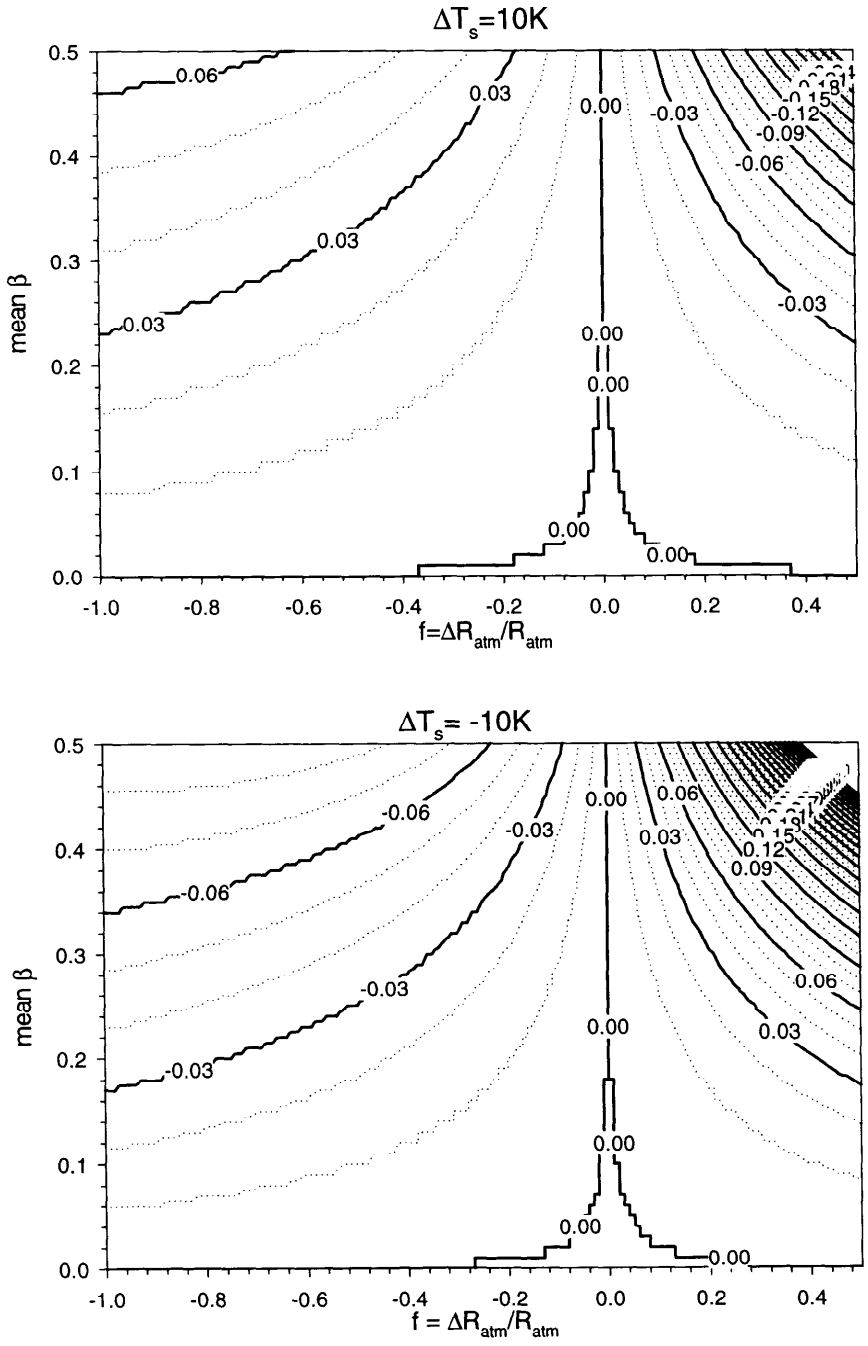

Figure 5. Variation of Δb in function of $\bar{\beta}$ and f for $\Delta T = \pm 10$ K and $\bar{T} = 300$ K.

again calculated using Modtran with two types of atmospheric profits: midlatitude summer and U.S. standard.

Sensitivity Analysis

Error Due to Method Simplification

In this section and in the following sections, we will take Channel 5 of TIMS as reference channel r and take $\varepsilon_{max}=0.98$ for each pixel. We denote E_{ir} as the relative emissivity of Channel i to Channel r, that is,

$$E_{ir}=\frac{\varepsilon_i}{\varepsilon_r^{nir}}\cong\frac{\varepsilon_i}{\varepsilon_r}. \qquad (14)$$

As an example, Figure 1a shows the histogram of $\Delta E_{15}=E'_{15}-E_{15}$, where E'_{15} is the relative emissivity derived from the first synthesized data set by the six methods described above and E_{15} is the emissivity ratio computed directly by the emissivity value from Eq. (14). Figure 1b depicts the standard deviation of ΔE for different channels of TIMS. Those figures show that:

a. The relative emissivity is underestimated by method a and an error of 0.6–1.1% in function of channel number is given by method a while methods RE and SR give an error of 0.1–0.3%.

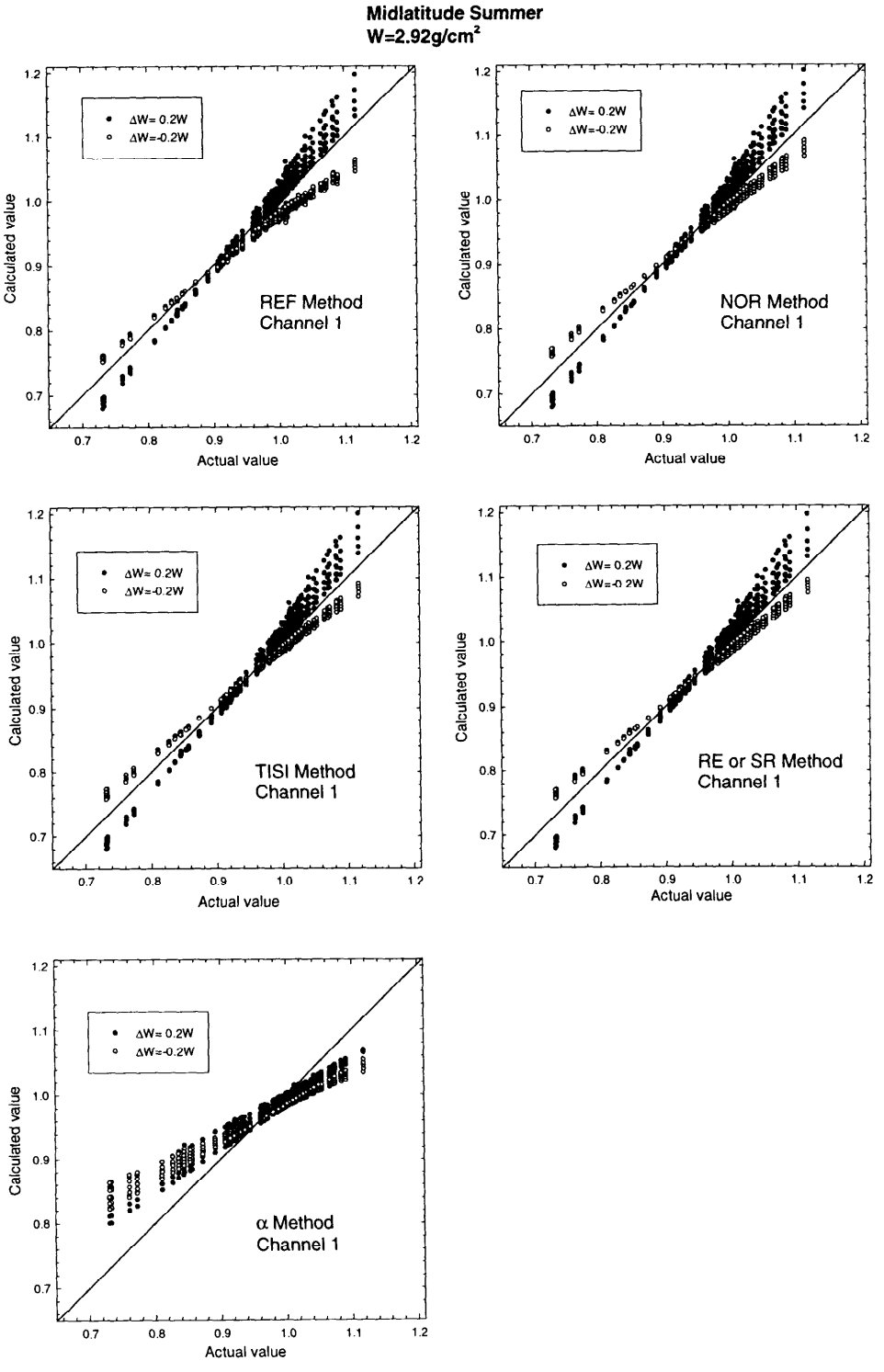

Figure 6. Effect of uncertainties of atmospheric parameters in atmospheric corrections on calculated relative emissivity. The abscissa represents the actual value E_{15} computed directly using emissivity values while the ordinate represents E'_{15} calculated from the simulated radiance with an error of ±20% on the actual total water vapor content W.

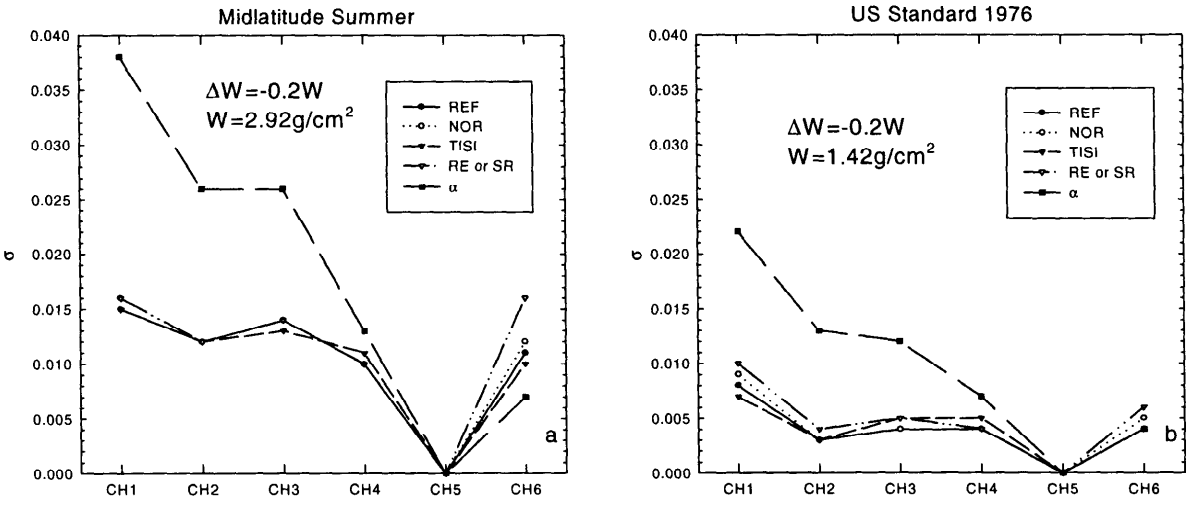

Figure 7. Standard deviation of $E_{i5}^{c}-E_{i5}$ calculated with the deviate atmosphere (water vapor content is underestimated by 20%) versus TIMS channels for two types of atmosphere: a) midlatitude summer; b) U.S. standard 1976.

b. Methods TISI, NOR, and REF give similar results as demonstrated by the second section.

Error Due to Instrumental Noise and Systematic Calibration Error

We calculated, from the data set including instrument noise and systematic calibration error, the relative emissitivity using the six methods. Table 1 shows the maximum absolute error (absolute ΔE) and the standard deviation of ΔE for NEΔT=0.1 K, 0.3 K, and for systematic calibration error ΔT_c=0 K. Because the position of Channel 1 is farthest from the reference Channel 5 and that of Channel 4 is nearest to Channel 5, the maximum of ΔE and minimum ΔE are expected respectively in Channels 1 and 4. Subtracting the error resulting from the model approximation given above, the error caused by instrumental noises is similar for all methods and varies from 0.002 to 0.005 for ΔT_c=0 K and for NEΔT=0.1 K to 0.3 K. We remarked from our calculations that the effect of systematic calibration error (ΔT_c=1 K) on relative emissivity extraction is about six times smaller than that of NEΔT= 0.1 K and therefore can be neglected. This is due to the fact that systematic calibration error affects the band brightness temperatures for all bands in the same direction and that for the case without atmosphere [see eq. (10)], the relative sensitivity E_{i5} is equal to $(T_{gi}/T_{gr})^m$, therefore, the error on E_{i5} is strongly reduced and can be neglected in comparison with the instrument noise.

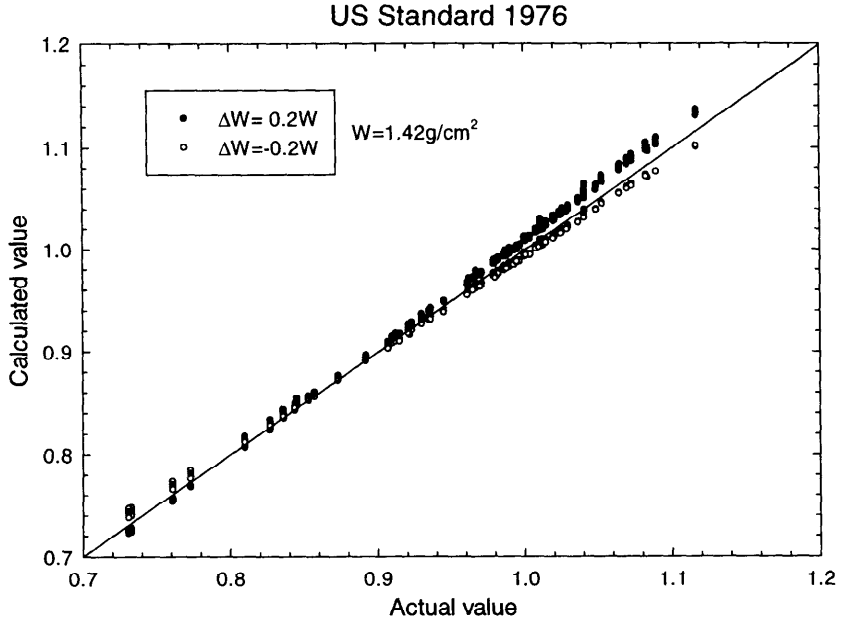

Figure 8. Same as Figure 6 but for U.S. standard atmosphere 1976 and TISI method.

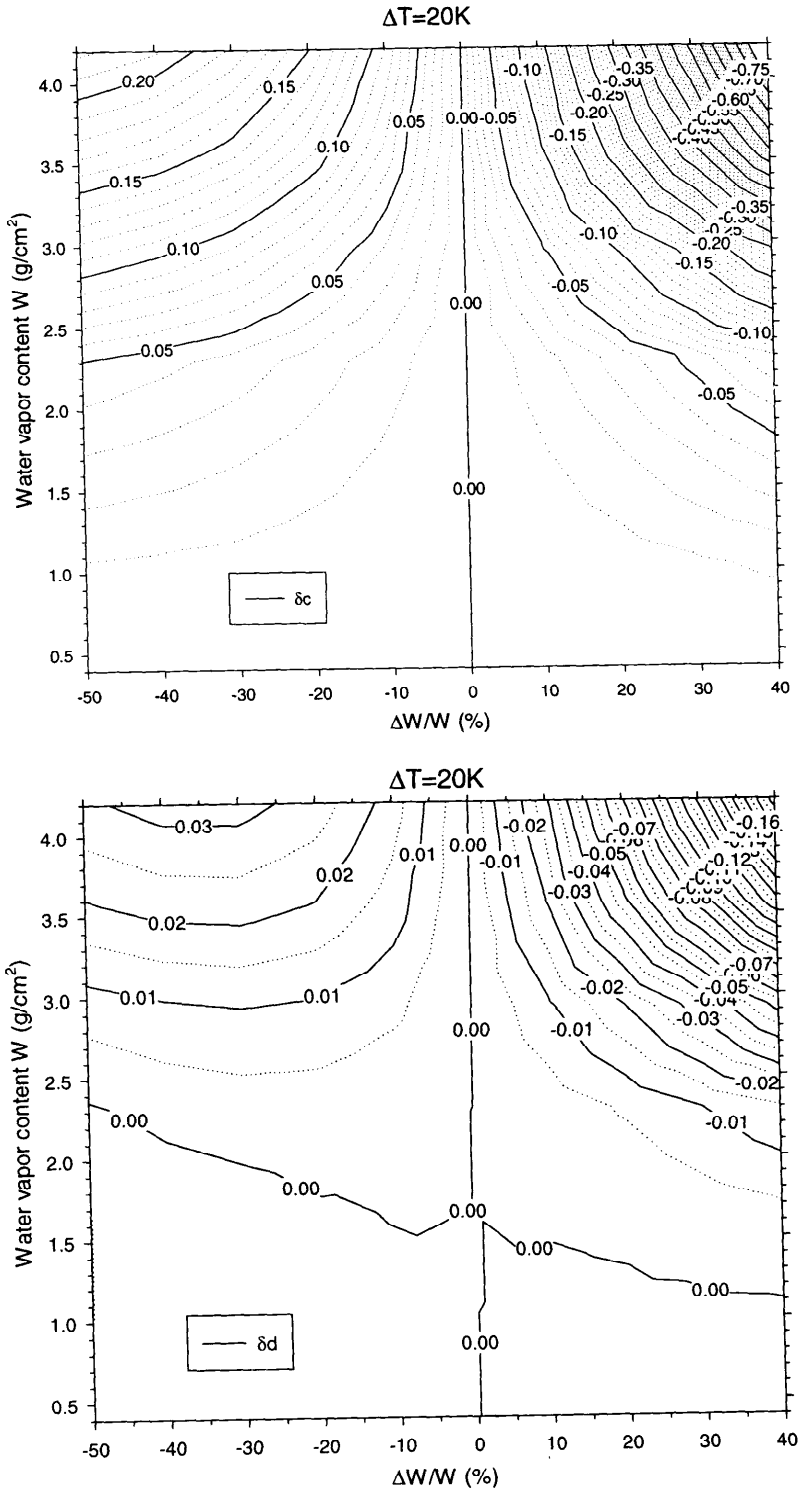

Figure 9. Variation of δc, δd for ΔT_s=20 K in function of the atmospheric water vapor content W and the relative error on W when the atmospheric corrections are performed.

Error Due to Uncertainties on the Estimation of Downwelling Atmospheric Radiance (R_{atd})

In this section, to analyze the sensitivity of different method to the error of R_{atd}, we applied the six methods to the data sets for radiance at surface level built up in a previous subsection with R_{atd} values changing from 0.8 to 1.2 times their actual values. As an example, Figure 2 shows the comparison of the relative emissivities E_{15}^c derived from simulated data set by six methods and E_{15} calculated directly from emissivity values [Eq. (14)], and Figure 3a displays the standard deviation of ΔE for all channels of TIMS.

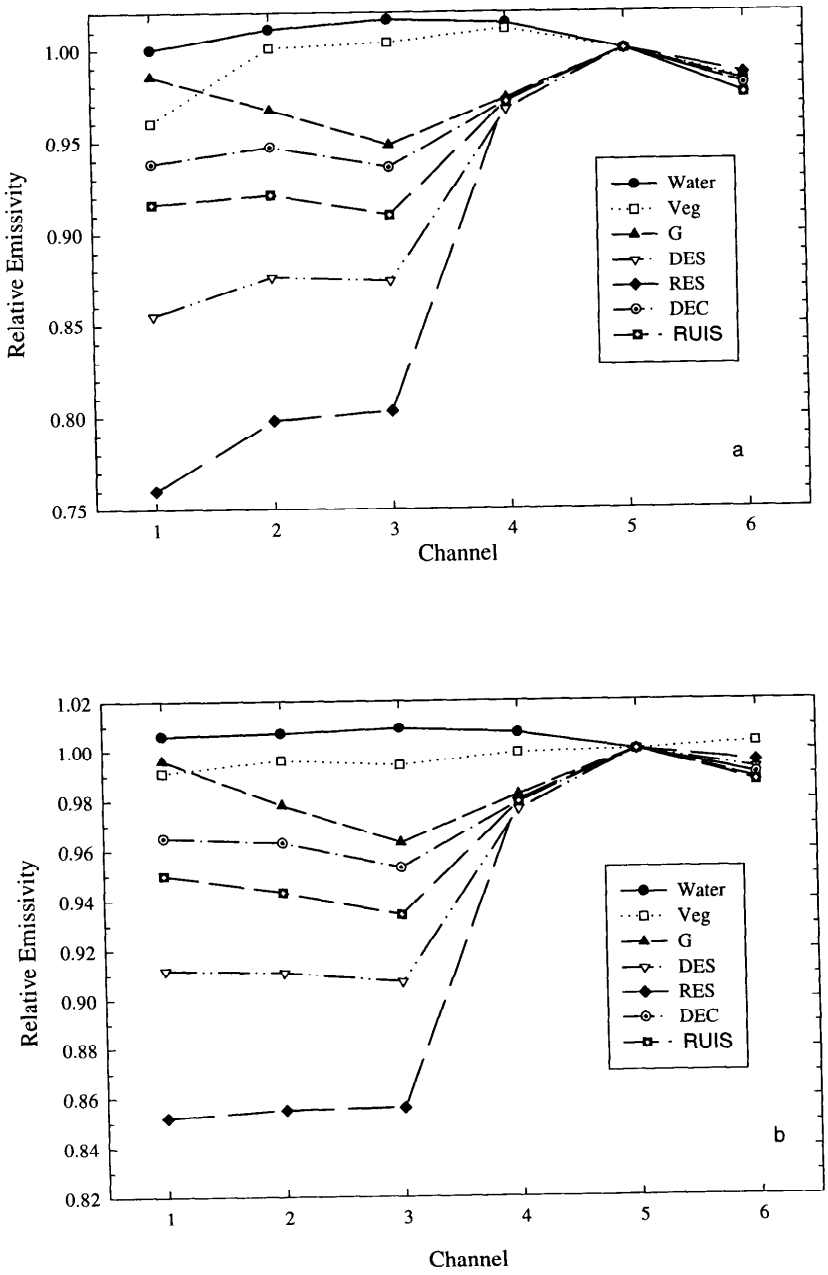

Figure 10. Relative spectral emissivity E^c_{i5} derived from real TIMS data by normalization method for different types of surfaces described in Table 2. The mineralogical and granulometric compositions of these types of soils have been given in Table 2 of Houssa et al. (1996): a) with radiosonde data; b) with modified radiosonde data.

We note that:

a. All methods, expect method *a*, give similar results: an error of −20% on $R_{atm\downarrow}$ leads to an error of 0.015 to 0.010 on relative emissivity, as displayed in Figure 3a. Those errors are smaller if the atmosphere is drier as this is the case for the U.S. standard atmospheric profile (W=1.42 g/cm^2) (Fig. 3b) instead of the midlatitude summer atmospheric profile (W=2.92 g/cm^2, Fig. 3a).
b. For TISI method, there is no impact of the error of $R_{atm\downarrow}$ on relative emissivity if the actual value of relative emissivity is greater than 1.0 (Fig. 2).
c. There exists a linear relationship between the estimated values of relative emissivity and its actual values as demonstrated by Figure 2. This linearity is much better when the atmosphere is drier as illustrated by Fig. 4.
d. The two linear regression lines are asymmetric to line 1:1. This means that the absolute error on relative emissivity due to a positive error of $R_{atm\downarrow}$ is not the same as that due to a negative value of error on $R_{atm\downarrow}$.

Those remarks can also be explained by the following mathematical analysis.

Table 2. Characteristics of Different Types of Surface Presented in Figure 10

Type of Surface	*Description*
Water	Dirty water
Veg	Vegetation
C	Crust with gravels (>2 mm)
DES	Crust not cultivated, slightly developed over the eolian sand
RES	Red eolian sand
DEC	Crust not cultivated, developed over organized surface
RUIS	Crust not cultivated, developed over sandy surface

Introducing $\Delta R_{atti\downarrow}$ into Eq. (7) or (11) and taking into account the definitions of β and $TISI_{ir}^{wa}$ given in Eqs. (6) and (10), we get the relative E^r

$$E^r=\frac{B_i(T_{gi})-(R_{atti\downarrow}+\Delta R_{atti\downarrow})}{B_i(T_g^{\max})-(R_{atti\downarrow}+\Delta R_{atti\downarrow})}=\frac{TISI_{ir}^{wa}-\beta_i(1+f_i)}{1-\beta_i(1+f_i)} \quad \text{with}$$

$$f_i=\frac{\Delta R_{atti\downarrow}}{R_{atti\downarrow}}, \tag{15a}$$

since

$$E=\frac{TISI_{ir}^{wa}-\beta_i}{1-\beta_i} \tag{15b}$$

from Eq. (15a), we get Eq. (16a) or Eq. (16b):

$$E^r=\frac{1-\beta_i}{1-\beta_i(1+f_i)}E-\frac{f_i\beta_i}{1-\beta_i(1+f_i)} \tag{16a}$$

or

$$E^r-E=b_i(T_s)(E-1) \quad \text{with}$$

$$b_i(T_s)=\frac{f_i\beta_i}{1-\beta_i(1+f_i)}. \tag{16b}$$

This illustrates the linear relationship between E^r and E as we displayed in Figure 2. In the strict sense, b_i depends on surface temperature T_s via β_i as shown in Eq. (6). If we approximate β_i by the first order of Taylor expansion and take into account Eq. (5c), we have

$$\beta_i=\frac{\bar{\beta}_i}{1+(n/\bar{T})\Delta T}, \tag{16c}$$

where $\bar{T}$ is the mean of surface temperature T_s, $\Delta T=T_s-\bar{T}$, and $\bar{\beta}_i$ is β_i corresponding to $\bar{T}$.

Thus, by combining Eqs. (16c) and 16b), the variation of $b_i(T_s)$ to its mean value $b_i(\bar{T})$ can be expressed as

$$\Delta b_i=b_i(T_s)-b_i(\bar{T})=\frac{f_i\bar{\beta}_i}{1-(1+f_i)\bar{\beta}_i+n\Delta T/\bar{T}}*\frac{n\Delta T/\bar{T}}{1-(1+f_i)\bar{\beta}_i}$$

From this expression, we remark that:

a. The smaller f_i $\bar{\beta}_i$ and ΔT are, the smaller Δb_i is. Noting that small $\bar{\beta}_i$ means dry atmosphere or/ and high surface temperature, and small ΔT means small thermal contrast in space.

b. The amplitude of Δb_i for $f_i>0$ (overestimation of

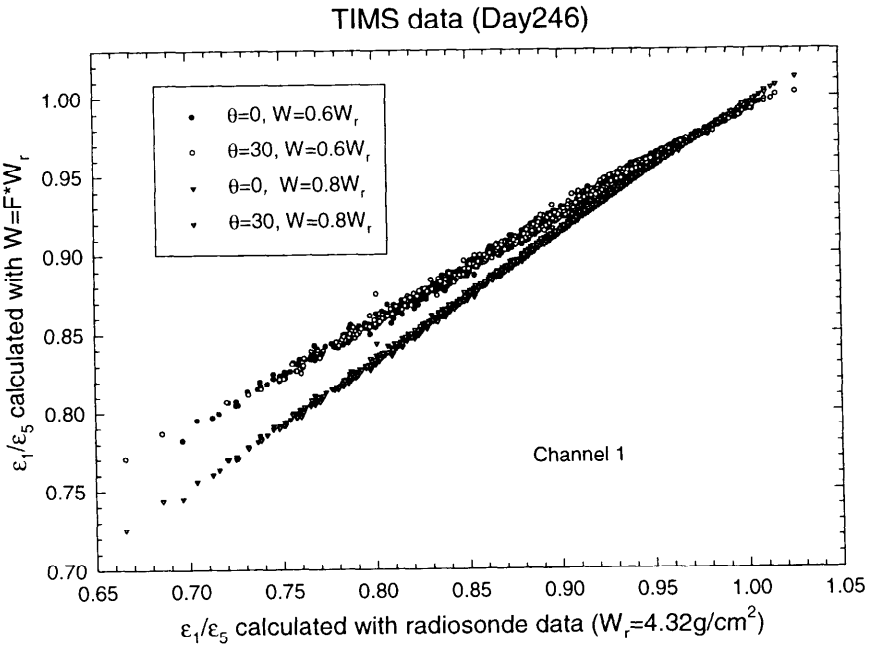

Figure 11. Illustration of linear relationship between E^r_{15} derived from TIMS data with radiosonde data (water vapor content $W=W_r=4.32$ g/cm^2) and E^r_{15} derived with deviate atmospheres ($W=0.6W_r$ and $W=0.8W_r$) for two view angles (nadir and 30°).

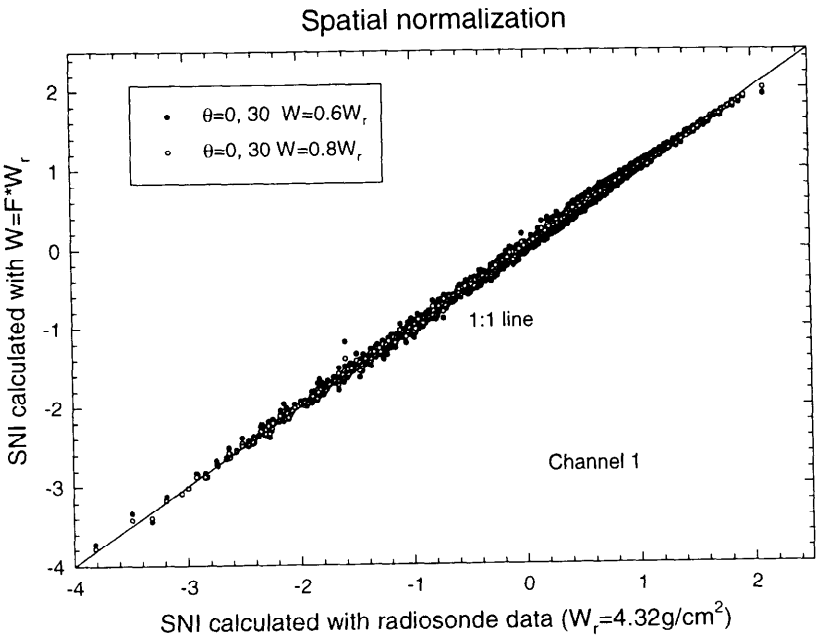

Figure 12. Demonstration of the independent of spatial normalization index (SNI) on the errors caused by atmospheric corrections or other errors having the linear property. Same data as displayed on Figure 11.

R_{atil}) and $\Delta T<0$ is larger than that for $f_i<0$ (underestimation of R_{atil}) and $\Delta T>0$.

The numerical computation shown in Figure 5 illustrates the variation of Δb predicted in function of $\bar{\beta}$ and f for $\Delta T=\pm 10$ K and $T=300$ K. It is interesting to note that:

a. The impact of f on Δb is pronounced when $f>0$ (overestimation of R_{atil}) as displayed by the upper right corner.
b. For small $\bar{\beta}$ ($\bar{\beta}<0.2$ for $\Delta T=\pm 10$ K) which corresponds to dry atmosphere or/and high surface temperature, Δb is smaller than ± 0.03 for almost all variations of f leading to an error on E^c less than $0.03*(E-1)$ according to Eq. (16b). As shown in Figure 2, for Channel 1, $|E-1|<0.3$ which means $\Delta E^c<1\%$. That is, under some circumstances, even if we neglect R_{atil} ($f=-1$) in our calculation, the influence of the variation of surface temperature on E^c is negligible and the linear relationship between E^c and E is almost independent of T_s.

Error Due to Uncertainties of Atmosphere in Atmospheric Corrections

Since the intent of this section it to explore the sensitivity of algorithms to residual, uncorrected atmospheric effects, we first perform the atmospheric correction on the simulated data built up previously, with the atmospheres differing from the atmospheres we have used earlier by 20% too little water and 20% too much water. Then we get the relative emissivities E^c_{ir} from the atmospherically corrected radiance and compared them with the relative emissitivities E_{ir} calculated directly from emissivity values [Eq. (14)]. As an example, Figure 6 shows this comparison for Channel 1 for midlatitude summer atmosphere, and Figure 7a displays the standard deviation of ΔE for all channels of TIMS for this atmosphere.

Some remarks can be made from those figures:

a. All methods, except method *a*, give the similar results and an error of -20% on water vapor content ($\Delta W=-0.58$ g/cm^2) leads to an error of 0.015 to 0.010 on relative emissivity as displayed in Figure 7a. Those errors are smaller if the atmosphere is drier as this is the case for the U.S. standard atmospheric profile ($W=1.42$ g/cm^2) (Fig. 7b) instead of the midlatitude summer atmospheric profile ($W=2.92$ g/cm^2, Fig. 7a).
b. The error on relative emissivity due to an error of -20% on water vapor content is similar to that due to an error of -20% on downwelling atmospheric radiance (comparison of Fig. 7 with Fig. 3). This shows that the impact of the downwelling atmospheric radiance error is important for relative emissivity retrievals.
c. There exists a linear relationship between the estimated values of relative emissivity E^c and its actual values E, especially for materials having the relative emissivity less than a fixed value, as demonstrated by Figure 6.
d. The dispersion from the linear regression line due to the variation of surface temperature is amplified for materials having the relative emissivity greater than the fixed value when the atmospheric effects are overestimated (Fig. 6, $\Delta W=0.2W$).
e. The fixed value depends on atmospheric water va-

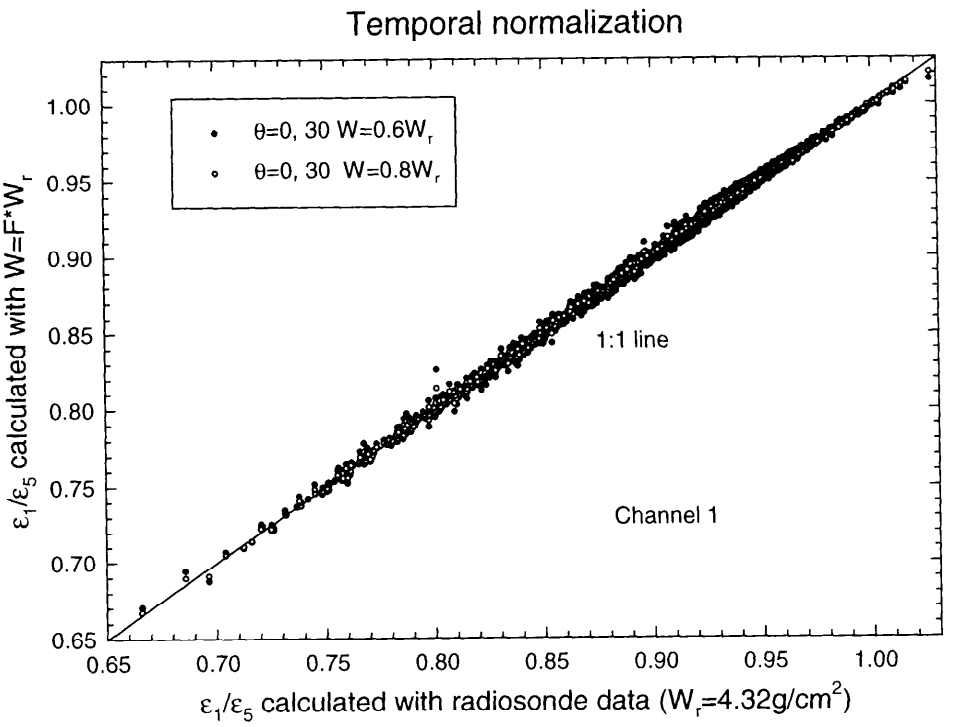

Figure 13. Illustration of the performance of the temporal normalization method to monitor the temporal variation of E. Same data as displayed in Figure 11.

por content. The drier the atmosphere is, the larger this fixed value is (comparison of Fig. 8 with Fig. 6).

f. The linear relationship is much better when the atmosphere is drier (comparison of Fig. 8 with Fig. 6).

g. The error on relative emissivity due to an overestimation of atmospheric effects is larger than that due to an underestimation of atmospheric effects.

Similar to the analysis in the preceding section, we denote the errors of surface brightness temperatures and R_{atti} generated by deviate atmosphere in atmospheric corrections as ΔT_{gi} (Channel i), ΔT_{gr} (Channel r), and ΔR_{atti}. From Eqs. (7) or (11), the relative emissivity is calculated by

$$E^c=\frac{B_i(T_{gi}+\Delta T_{gi})-(R_{atti\downarrow}+R_{atti\uparrow})}{B_i(T_{gr}+\Delta T_{gr})-(R_{atti\downarrow}+R_{atti\uparrow})}$$

Taking the first order of Taylor approximation of B_i and denoting $L_k=\partial B_k(T_{gk})/\partial T/B_k(T_{gk})=n_k/T_{gk}$ ($k=i$ or r), we have

$$E^c=\frac{TISI_{ir}^{wa}(1+L_i\Delta T_{gi})-\beta_i(1+f_i)}{1+L_r\Delta T_{gr}-\beta_i(1+f_i)}.$$

Replacing $TISI_{ir}^{wa}$ by Eq. (15b), E^c becomes

$$E^c=\frac{(1-\beta_i)(1+L_i\Delta T_{gi})}{1+L_r\Delta T_{gr}-\beta_i(1+f_i)}E+\frac{\beta_i(L_i\Delta T_{gi}-1)}{1+L_r\Delta T_{gr}-\beta_i(1+f_i)} \quad (17a)$$

or

$$E^c-E=c_i(E-1)+d_i \quad (17b)$$

with Eq. (17c)

$$c_i=\frac{\beta_i(f_i-L_i\Delta T_{gi})+L_i\Delta T_{gi}-L_r\Delta T_{gr}}{1+L_r\Delta T_{gr}-\beta_i(1+f_i)} \quad \text{and}$$

$$d_i=\frac{L_i\Delta T_{gi}-L_r\Delta T_{gr}}{1+L_r\Delta T_{gr}-\beta_i(1+f_i)}. \quad (17c)$$

Expression (17a) or (17b) illustrates the linear relationship between E^c and E as we showed in Figure 6. One should keep in mind that the slope c_i and the offset d_i depend on surface temperature via β_i, ΔT_{gi}, and ΔT_{gr}. From expression (17b), the variation of E^c (δE^c) due to that of surface temperature may be written as

$$\delta E^c=\delta c_i(E-1)+\delta d_i. \quad (17d)$$

Figure 9 displays by numerical simulation δc_i, δd_i for $\Delta T_s=20$ K in function of the atmospheric water vapor content W and the relative error on W committed when we perform the atmospheric corrections. This figure shows that:

a. If $E<1$, there is some compensations between the first term and the second term in the right-hand side of Eq. (17d), otherwise the variation of E^c on surface temperature is amplified because δc_i and δd_i are the same sign. In the case where $E=1-\delta d_i/\delta c_i$, $\delta E^c=0$.

b. δc_i, δd_i are pronounced when the atmospheric effects are overestimated ($\Delta W/W>0$), but their combination effect on δE^c largely decreases when $E<1$ as explained in a.

c. For $W<2.0$, the variation of E^c due to that of sur-

face temperature is less than 1% for $|\Delta W/W|<40\%$ and $E<1$ (E between 0.7 and 1.0).

In conclusion, one can say that:

a. All methods are very sensitive to the uncertainties of atmosphere. Considering the overall error, the TISI and normalization methods are slightly superior to other methods. Since the concept of normalization method is straight and simple, we select it to deal with the real data in the following section.
b. The relative emissivity E^r calculated with deviate atmosphere is linearly related to the actual value E. This is a very important property that we will explore in the following section.

APPLICATION TO REAL TIMS DATA

Data Collection

The TIMS data were acquired during Hapex-Sahel experiment on 2 September 1992 at 13 h 36. The flight height was 600 m. The atmospheric profiles (PTU) were measured at 13 h by CNRM just one half hour before the airplane passed. The total column water vapor content (to infinity) was 4.32 g/cm^2 while the total water vapor up to airplane height was 0.94 g/cm^2. TIMS data of flight 4 were used in this study.

Preliminary Results

Sample Spectral Analysis

After the data calibration was performed with the two blackbodies on board, the count number was converted to brightness temperature. From this brightness temperature, the relative emissivity was derived using the normalization method in which the maximum emissivity among six channels for one pixel was set to 0.98 and the atmospheric quantities (τ_i, R_{atti} and R_{atti}) were calculated by Modtran 3.5 with the radiosonde data.

As an example, Figure 10a shows the relative spectral emissivity shape E^r_{i5} for different types of surface whose characteristics are shown in Table 2. Each value presented in this figure is the average of about 15∘15 pixel values on the same type of surface. We note that the relative emissivity curve for vegetation is not as flat as it should be, particularly, the relative emissivities in Channels 1 and 6 are smaller than the others. We thought this abnormality is caused by the imperfect atmospheric corrections due to uncertainties of atmospheric profiles. Therefore, we modified the temperature and humidity profiles using two rules:

a. Keep the adiabatic rate unchanged and modify the air temperature (T_a) by adding a constant ΔT_a up to 8 km.
b. Modify the humidity (Hum) by a factor F: Modified Hum=Measured Hum∘F.

The aim of those modifications is to get the emissivity curve flat. In order to accomplish this objective, we first selected a box of 20∘20 pixels of vegetation in the middle of image and took the average of their brightness temperatures to reduce the instrumental noise. Then, considering the fact that vegetation is a good grey body, a least-square method was used to get four unknowns (one surface emissivity, one surface temperature, one ΔT_a, and one F) from six brightness temperatures (six equations, each for one channel of TIMS). The results we got for vegetation are $\varepsilon=0.964$, $T_s=298.7$, $\Delta T_a=-3.9$ K, and $F=0.77$.

Instead of using the radiosonde data, we used the modified profiles to get the relative emissivity for above samples. Figure 10b displays those results. We note that

a. The vegetation spectral shape is largely improved although this sample is not the sample we took to modify the atmospheric profiles.
b. The differences of relative emissivity between Channels 1 and 3, and between Channels 3 and 4 are very useful to discriminate the different types of surface.

Verification of Linear Effects Due to the Imperfect Atmospheric Corrections

The purpose of this subsection is to check whether the linear relationship between E^r and E we found above exists on real data. To do this, we calculated respectively the relative emissivity E^r_{i5} from TIMS data using the radiosonde data and the relative emissivity using the modified atmospheric profiles (humidity has been modified by a factor of 0.6 and 0.8 and $\Delta T_a=0$ K). If we assume that E^r_{i5} derived with radiosonde data is the value of true E_{i5}, the linear correlation between those relative emissivities and those derived with the modified profiles should exist. Figure 11 shows those correlation for two columns of image. Those two columns correspond respectively to two view angles: 0° and 30°. We note that at least for this image:

a. The linear correlation exists.
b. The slope and offset of those linear relations are almost independent on view angle.

Possible Error Correction Methods

As illustrated above, the effects of error in atmospheric corrections on relative emissivities are linear. Based on this property and assuming that there is no spatial variation in the atmospheric conditions over the study region in the image, three methods are proposed to correct for those effects. They refer to the reference point calibration method, the spatial normalization method, and the temporal normalization method. In the following, the subscript indicating the channel number will be omitted.

Reference Point Calibration Method: If the observations are taken on the ground level and if the values of E for one reference point are known *a priori* from the

field measurements or from the other ways, according to Eq. (16b), the offset of the linear relationship between E^c and E is $-b$ which can be obtained by

$$b=(E^c-E)/(E-1)$$

and the slope is $1+b$. Noting that the E value of reference point cannot be close to unity.

After knowing b, the values of E for other points in the images can be easily derived by inverting Eq. (16b), that is,

$$E=(E^c+b)/(1+b).$$

If the observations are taken from space, according to Eq. (17b), two reference points are needed to get the slope $(1+c)$ and the offset $(d-c)$ with which the E values for other points can be calculated from

$$E=(E^c+c-d)/(1+c).$$

This method can be used to obtain the actual E values, but it needs to know *a priori* the E values for at least one reference point which is generally seldom available.

Spatial Normalization Method: Some applications such as classification and discrimination of different types of surfaces need only some indices characterizing the surface intrinsic spectral property. Based on the linearity of errors due to the imperfect atmospheric corrections and taking into account the spatial information, an index called spatial normalization index (SNI) can be constructed by

$$SNI=\frac{E^c-\overline{E^c}}{\sigma_{E^c}}, \tag{18}$$

where $\overline{E^c}$ and σ_{E^c} are respectively the mean and the standard deviation of E^c observed on a zone. By considering Eq. (17b) into Eq. (18), SNI becomes Eq. (19):

$$SNI=\frac{(1+c)(E-\overline{E})}{(1+c)\sigma_E}=\frac{E-\overline{E}}{\sigma_E}, \tag{19}$$

which means that the index SNI is independent on the errors caused by atmospheric corrections or other errors having the linear property.

It should be noted that this index is scene-dependent and it cannot be used to monitor the temporal variation of surface spectral properties; thus it is impossible to perform the comparison between different images. As an example, SNI was applied to the data displayed in Figure 11. The results are shown in Figure 12 in which the abscissa represents the SNI obtained with the radiosonde data while the ordinate represents SNI calculated with the deviate atmospheres. This figure illustrates the performance of the spatial normalization method.

Temporal Normalization Method: This method is also based on the linear relationship between E^c and E. Unlike the reference point calibration method, this method does not need to know the exact values of E for reference points. One needs only to choose a time I as reference time, and select some samples in the image for which no time variation of relative emissivity is assumed, then the linear regression on those selected points are processed between time I (reference time) and each other time J to get the slope $slp(J)$ and the offset $ofst(J)$. Under the assumption that the effects of spatial variation in the atmospheric conditions at times I and J are not larger than the effect of instrument noise, with these slope and offset, $E^c(J)$ for the entire data set at time J can be normalized to $E(J\rightarrow I)$ by

$$E(J\rightarrow I)=(E^c(J)-ofst(J))/slp(J), \tag{20}$$

where $E(J\rightarrow I)$ is the relative emissivity at time J normalized to that of reference time I, that is, the relative emissivity which would have been obtained at time J with the atmosphere at time I. According to Eq. (17b), $slp(J)=1+c$, $ofst(J)=d-c$.

As expected, the linear errors at time J with respect to reference time I are suppressed by Eq. (20); therefore the monitoring of the temporal variation of E becomes possible using temporal normalization methods. If $E(J\rightarrow I)\neq E^c(I)$, one can say the surface spectral properties have been changed during times I and J; otherwise they remain constant.

As we did for spatial normalization method, we take the data displayed in Figure 11 as an example and suppose the TIMS data be acquired three times over the same region with the same surface and atmosphere (in fact, we have only one image). We choose E^c obtained with radiosonde data as $E^c(I)$ and the two others ($F=0.6$ and 0.8, $\Delta T_a=0$ K) as $E^c(J)$. Then applying the temporal normalization to these data, we got $E(J\rightarrow I)$. Since we have only one image, the surface properties are the same for three times, as we expected, representation of $E(J\rightarrow I)$ in function of $E^c(I)$ should be laid on 1:1 line as demonstrated by Figure 13.

CONCLUSION

The sensitivity of six published methods for extracting relative spectral emissivity information from thermal infrared multispectral data to different sources of error has been analyzing using the simulated data. The results of this analysis show that all methods are nearly insensitive to instrumental noise and systematic calibration error but are very sensitive to the atmospheric correction errors particularly when the atmospheric effects are overcorrected for. Considering the overall error, the TISI and normalization methods are slightly superiors to other methods, thus we recommend users to use those two methods for their proper applications. The study also shows that the relative emissivity derived with deviate atmosphere is linearly related to its actual value. Based on this property, we propose three methods to correct for the errors caused by atmospheric corrections under horizontally invariant atmospheric conditions. A practical analysis with the real TIMS data acquired for Hapex-Sahel experiment in 1992 supports the simulation results.

We would like to express our gratitude to Dr. T. J. Schmugge at USDA Hydrology Laboratory, Beltsville for providing us the TIMS data and P. Bessemoulin of CNRM for the radiosoundings. We would also like to think Dr. A. Gillespie and other anonymous reviewers for very helpful and stimulating comments. Dr. Z.-L. Li wishes to thank Professor M. P. Stoll at LSIIT and the CNRS for allowing him to leave Strasbourg in 1998 and Dr. Wan at UCSB for providing him the financial support during his stay at UCSB. Dr. Wan is supported by the NASA Contract NAS5-31370.

REFERENCES

Barducci, A., and Pippi, I. (1996), Temperature and emissivity retrieval from remotely sensed images using the "grey body emissivity" method. *IEEE Trans. Geosci. Remote Sens.* 34:681–695.

Becker, F., and Li, Z.-L. (1990). Temperature-independent spectral indices in thermal infrared bands. *Remote Sens. Environ.* 32:17–33.

Becker, F., and Li, Z.-L. (1995). Surface temperature and emissivity at various scales: definition, measurement and related problems. *Remote Sens. Rev.* 12:225–253.

Gillespie, A. R. (1985), Lithologic mapping of silicate rocks using TIMS. In *The TIMS Data Users' Workshop*, JPL Publication 86-38, Jet Propulsion Laboratory, Pasadena, CA, pp. 29–44.

Gillespie, A. R., Rokugawa, S., Hook, S., Matsunaga, T., and Kahle, A. B. (1996), Temperature/emissitivity separation algorithm theoretical basis document, version 2.3, Jet Propulsion Laboratory, Pasadena, CA, August, http://asterweb.jpl.nasa.gov/asterhome/atbd/ATBD-AST-03.doc.

Gillespie, A. R., Rokugawa, S., Matsunaga, T., Cothern, J. S., Hook, S. and Kahle, A. B. (1998), A Temperature and emissivity separation algorithm for Advanced Spaceborne Thermal Emission and Reflection Radiometer (ASTER) images. *IEEE Trans. Geosci. Remote Sens.* 36:1113–1126.

Houssa, R., Pion, J.-C., and Yesou, H. (1996). Effects of granulometric and mineralogical composition on spectral reflectance of soils in a Sahelian area. *ISPRS J. Photogramm. Remote Sens.* 51:284–298.

Kahle, A. B., and Goetz, A. F. H. (1983), Mineralogic information from a new airborn Thermal Infrared Multispectral Scanner. *Science* 222:24–27.

Kahle, A. B., Madura, D. P., and Soha, J. M. (1980), Middle infrared multispectral aircraft scanner data: analysis for geological applications. *Appl. Opt.* 19:2279–2290.

Kealy, P. S., and Gabell, A. R. (1990), Estimation of emissivity and temperature using alpha coefficients. In *Proceedings of the Second TIMS Workshop*, JPL Publication 90-55, Jet Propulsion Laboratory, Pasadena, CA, pp. 11–15.

Kneizys, F. X., Abreu, L. W., Anderson, G. P., et al. (1996), The MODTRAN 2/3 Report and LOWTRAN 7 MODEL, Ontar Corporation, North Andover, MA.

Palluconi, F., and Meeks, G. R. (1985), *Thermal Infrared Multispectral Scanner (TIMS): An Investigator's Guide to TIMS Data*, JPL Publication 85-32, Jet Propulsion Laboratory, Pasadena, CA.

Prince, S. D., Kerr, Y. H., Goutorbe, J. P., et al. (1995), Geographical, biological, and remote sensing aspects of the Hydrologic Atmospheric Pilot Experiment in the Sahel (HAPEX-Sahel). *Remote Sens. Environ.* 51:215–234.

Realmuto, V. J. (1990), Separating the effects of temperature and emissivity: emissivity spectrum normalization. In *Proceedings of the Second TIMS Workshop*, JPL Publication 90-55, Jet Propulsion Laboratory, Pasadena, CA, pp. 23–27.

Salisbury, J. W., and D'Aria, D. M. (1992), Emissivity of terrestrial materials in the 8–14 μm atmospheric window. *Remote Sens. Environ.* 42:83–106.

Stoll, M. (1993), Restitution de la temperature de surface par teletedection aeroportee dans le cadre de Hapex-Mobilhy, Ph.D. thesis, Paul Sabastier University, Toulouse, France.

Vincent, R. K., and Thomas, F. J. (1972), Rock-type discrimination from ratioed infrared scanner images of Pisgah Crater, California. *Science* 175:986–988.

Wan, Z., and Snyder, W. (1996), MODIS land surface temperature algorithm theoretical basis document, version 2.3, ICESS/UCSB, December, http://modarch.gsfc.nasa.gov/MODIS/ATBD/atbd_mod11.pdf.

Wan, Z., and Li, Z. L. (1997), A physics-based algorithm for retrieving land-surface emissivity and temperature from EOS/MODIS data. *IEEE Trans. Geosci. Remote Sens.* 35: 980–996.

Watson, K. (1992a), Two-temperature method for measuring emissivity. *Remote Sens. Environ.* 42:117–121.

Watson, K. (1992b), Spectral ratio method for measuring emissivity. *Remote Sens. Environ.* 42:113–116.